Chinese Journal of Physics 87 (2024) 646–664

Contents lists available at ScienceDirect

Chinese Journal of Physics

journal homepage: www.sciencedirect.com/journal/chinese-journal-of-physics

Micropolar nanoparticles flow on a stretching/shrinking sheet with multiple slips

U.S. Mahabaleshwar [a], G.P. Vanitha [a,b], L.M. Pérez [c], H.F. Oztop [d,e,f,*]

[a] Department of Studies in Mathematics, Davangere University, Shivagangothri, Davangere, 577 007, India
[b] Department of Mathematics, Siddaganga Institute of Technology, Tumkur, 572 103, India
[c] Departamento de Física, FACI, Universidad de Tarapacá, Casilla 7D, Arica, Chile
[d] Department of Mechanical and Nuclear Engineering, College of Engineering, University of Sharjah, 27272 Sharjah, United Arab Emirates
[e] Department of Mechanical Engineering, Technology Faculty, Fırat University, Elazığ, Turkey
[f] Department of Medical Research, China Med. University Hospital, China Med. University, Taichung, Taiwan

ARTICLE INFO

Keywords:
Micropolar fluid
Multiple slips
Chemical reaction
Nanoparticles
Stretching/shrinking sheet
Analytical solution

ABSTRACT

The purpose of this paper is to examine the flow of micropolar fluid containing ternary nanoparticles, with multiple slips over a stretching/shrinking sheet. Also, the influences of internal radiation and with the first order chemical reaction are examined to study the fluid properties. Mathematical modeling for the defined problem is framed and yields coupled nonlinear PDEs which are then reduced to nonlinear ODEs by choosing suitable similarity variables. The resulting ODEs are solved by analytical technique and solution is represented as an incomplete gamma function and a hypergeometric function. The regulating parameters, such as Eringen parameter, chemical reaction parameter, inverse Darcy number, Prandtl number and radiation parameter impact are examined for the profiles of velocity, microrotation, energy and concentration of the fluid through graphs. Furthermore, the skin friction drag of the defined flow is also discussed. This investigation reveals the existence of multiple solutions for the case of shrinking and for the case of stretching it shows a unique solution. Also, the tri-hybrid nanofluid flow velocity is found to increase and decrease for the first and second solutions respectively. The velocity, energy and concentration of the flow are found to decrease due to slip conditions.

1. Introduction

Due to its growing practical significance and applicability in numerous industrial processes, the analysis of NNFs has garnered significant interest from researchers in recent years. Real-world industrial uses for these fluids include food processing, oil extraction and polymer engineering. The intricate rheological behavior that industrially important fluids exhibit at the micro and nanoscales has been observed to defy description by Navier's governing equations of traditional hydrodynamics. Because of these, a number of micro-continuum theories have been developed, including those based on micro and micropolar fluids, deformable fluids, polar fluids and anisotropic fluids, based on various physical properties. On the other hand, the variety of fluid properties found in nature, but not every NNF can be described by one constitutive model. As a result, various models of NNFs, including the Maxwell fluid, micropolar fluids, Jeffery fluid, Casson fluid and power law fluid, have been developed by Chen et al. [1]. In their investigation, small traces of fluids

* Corresponding author.
E-mail address: hfoztop1@gmail.com (H.F. Oztop).

https://doi.org/10.1016/j.cjph.2023.12.014
Received 22 August 2023; Received in revised form 11 December 2023; Accepted 12 December 2023
Available online 18 December 2023

Nomenclature

aAcceleration rate Acceleration rate$(1/s)$
c, CConcentration parameters Concentration parameters(mol/m^3)
$(C)_p$Specific heat Specific heat(J/kgK)
DMass diffusion parameter Mass diffusion parameter(m^2/s)
dStretch/shrink parameter Stretch/shrink parameter(-)
$1/(Da)$Darcy number inverse Darcy number inverse(-)
EEringen factor Eringen factor(-)
FNon-dimensional velocity function Non-dimensional velocity function(-)
GNon-dimensional microrotation function Non-dimensional microrotation function(-)
kPermeability parameter Permeability parameter (m^2)
K_1Dimensionless chemical reaction parameter Dimensionless chemical reaction parameter(-)
NVelocity parameter due to micro rotation Velocity parameter due to micro rotation(rad/s)
RRadiation number Radiation number(-)
Re_xReynolds number Reynolds number(-)
SCSchmidt number Schmidt number(-)
u, vDimensional velocity elements Dimensional velocity elements(m/s)
U, VNon-dimensional velocity components Non-dimensional velocity components (-)
v_wVariable mass velocity Variable mass velocity (m/s)
$V_c\left(=-\frac{v_w}{\sqrt{av}}\right)$Suction/injection parameter $\left(=-\frac{v_w}{\sqrt{av}}\right)$Suction/injection parameter(-)
(x, y)Dimensional coordinates of the plane Dimensional coordinates of the plane(m)
X, YDimensionless coordinates of the plane Dimensionless coordinates of the plane(-)

Greek Symbols
β, Γ, ζParameters Parameters(-)
εPorosity parameter Porosity parameter(-)
κViscosity coefficient Viscosity coefficient$(Pa\ s)$
νViscosity (Kinematic) Viscosity (Kinematic)(m^2/s)
μViscosity (Dynamic) Viscosity (Dynamic)$(Pa\ s)$
ρDensity Density(kg/m^3)
ϕVolume fraction Volume fraction(-)
ΦNon-dimensional concentration variable Non-dimensional concentration variable(-)
ΨStream function Stream function(-)

Subscripts
tnfTernary nanofluid Ternary nanofluid(-)
wWall state Wall state(-)
∞Infinite boundary state Infinite boundary state(-)
fPure fluid Pure fluid(-)

Abbreviation
BLFBoundary layer flow Boundary layer flow(-)
FSFirst solution First solution(-)
MHDMagnetohydrodynamics Magnetohydrodynamics(-)
MPFMicropolar fluid Micropolar fluid(-)
NFNewtonian fluid Newtonian fluid(-)
NNFNon-Newtonian fluid Non-Newtonian fluid(-)
NSNo-slip No-slip(-)
ODEsOrdinary differential equations Ordinary differential equations(-)
PDEsPartial differential equations Partial differential equations(-)
SSSecond solution Second solution(-)
2DTwo-dimensional Two-dimensional(-)
SBStefan-Boltzmann Stefan-Boltzmann(-)

containing polymeric additives are considered. The investigators [2,3] found that the fluids exhibit a decrease in friction close to the rigid body. Eringen [4,5] created the governing model for the theories of thermo-micropolar and micropolar fluids as a result. MPFs, which include microstructure and play a significant role in Navier's model, are an essential component of NNF dynamics. The theory

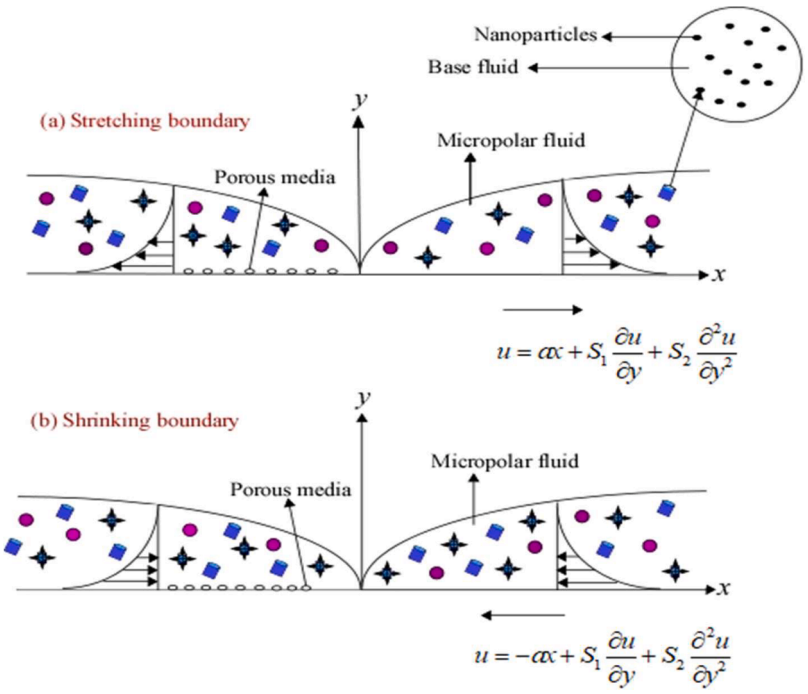

Fig. 1. Schematic diagram of the problem.

states that every fluid component has two kinds of degrees of freedom: one is rotational and translational, which determine velocity, and the other is rotation/stretch, which enables the particles to experience separate intrinsic spin and heterogeneous deformation. These fluids enable a mathematical framework to analyze a variety of intricate and sophisticated fluid dynamics, including those of suspension solutions, blood flow ability, and colloidal fluids. Polymeric liquids, suspensions of liquids, blood (animal's), liquid crystallization, dusty clouds, colloidal fluids, etc. all contain MPFs and are studied by Ahmadi [6] and Hayat *et al.* [7]. Investigators interest in understanding it has also increased because of its use in various industrial processes, including the excrescence of polymers, unusual lubricant flow, colloidal mixtures, and also metallic plates cooling in water baths investigated by Rahman [8]. Further, Lukaszewicz [9], Maryam et al. [10]., Nadeem et al. [11]., Ishtiaq et al. [12]., Usafzai et al. [13,14]. and Merkin et al. [15]. provided a thorough overview of the physics and uses of MPFs.

The investigation of the flow characteristics caused by stretched surfaces is crucial to industrial processes. It includes the manufacturing of plastic sheets through aerodynamic extrusion, wire drawing, paper, glass fibre, and hot rolling. Crane [16] carried out the ground-breaking exertion of an incompressible viscous continuous flow on the boundary layer which is caused by a linearly extending sheet. Energy and mass transport over stretching sheets with blowing or suction were included in Gupta and Gupta's [17] extension of the study. Haq et al. [18]. conducted a numerical investigation of the flow of the micropolar nanofluid through internal buoyancy effects and radiation. In reality, the MPF flow characteristics have been examined by numerous researchers in a variety of contexts [19–21]. Mahabaleshwar et al. [22,23]. conducted an analytical investigation of the mixed convection of angled MHD flow across a stretched sheet. In three dimensions, Chamkha *et al.* [24] quantitatively examined the circulation of a MPF caused by a flat stretching surface that is not dependent on time. Bhatti et al. [25]. Selimefendigil and Oztop [26,27] investigated the thermal properties of the flow due to nanoparticles and listed their applications in cooling systems, packed bed systems and solar collectors. Many researchers [28–33] worked on nanofluid flow and reported the importance of the inclusion of nanoparticles. Due to their significance in chemical reaction processes and industries of hydrometallurgy, such as food fermentation, the manufacture of polymers and ceramics, and the analysis of mass and energy transmission in a BLF while incorporating chemical reaction, is of practical significance and is examined by Das [34] and Mishra et al. [35]. Bhattacharyya and Layek [36] investigated an MHD flow that involves chemical processes and diffusion through a permeable flat plate with blowing/suction.

The aforementioned studies have focused only on NF and NNF flow and energy transfer issues using the NS condition at the boundary (which means fluid sticks to the boundary surface). The slip conditions may need to be used in place of the NS boundary condition for various practical flow issues because this assumption does not always hold true in practice. Velocity slip is the non-adherence of a fluid to a solid boundary. The non-equilibrium area near the surface is better described by the temperature jump and velocity slip conditions, which signifies the interruption in the transmission variable at the surface. Since there are many NF/NNF, including particle fluids like emulsions and polymer solutions, where there is a slip between the fluid and the wall, slip condition flow problems are particularly important in the cases of static and moving boundaries by Wang [37]. The polishing of prosthetic heart valves and interior cavities is one example of how such technological research is put to use by Mukhopadhyay [38]. Anderson [39]

investigated the slip condition imposed on a NF flow across a linearly stretched sheet in order to achieve this. The effect of radiation on MHD flow via a stretching sheet by considering heat source/sink and varying viscosity with slip conditions was examined by Devi *et al.* [40]. In an MHD flow across a stretched surface with slip conditions, Kemparaju et al. [41] investigation looked at heat transfer.

In view of the literature survey, the investigation of MPF flow with heat and mass transfer containing ternary nanoparticles has not been analyzed. Therefore, the scope of the article is to analyze the impact of multiple slips on flow, energy and concentration of MPF containing ternary nanoparticles that flows across a stretching/shrinking sheet with the effect of radiation and chemical reactions of first order. Analytical solutions are extracted and expressed as incomplete gamma functions and hypergeometric functions. The present analysis is compared with the numerical solution obtained by Fatunmbi and Adeniyan [42].

2. Model description and solution technique

The investigation deals with the steady, 2D MPF flow containing nanoparticles, past the porous stretching/shrinking sheet with multiple slips to study the impact of radiation, mass transpiration and chemical reactions. Fig. 1 explains the fluid motion caused by shrinking/ stretching sheet.

The framework of the defined problem is as follows:

■ Equation of Continuity:

$$\nabla.\,\vec{q} = 0, \tag{1}$$

■ Equation of Linear momentum:

$$\rho_{tnf}[(\vec{q}.\nabla)\vec{q}] = -\nabla p + \rho_{tnf}\vec{g} - \frac{\mu_{tnf}}{k\,a}\vec{q} + (\kappa + \mu_{tnf})\nabla^2\vec{g} + \kappa(\nabla \mathrm{x}\,\vec{\omega}), \tag{2}$$

■ Equation of Microrotation:

$$\rho_{tnf}[(\vec{q}.\nabla)\vec{\sigma}] = \gamma_{tnf}\,\nabla^2\vec{\sigma} + \kappa(\nabla \mathrm{x}\,\vec{q} - 2\vec{\sigma}), \tag{3}$$

■ Equation of Energy:

$$(\vec{q}.\nabla)T_1 = \alpha_{tnf}\nabla^2 T_1 - \frac{1}{(\rho C_p)_{tnf}}(\nabla.q_r), \tag{4}$$

■ Equation of concentration:

$$(\vec{q}.\nabla)c = D\,\nabla^2 c, \tag{5}$$

here, $\vec{q} = (u, \mathrm{v}, 0)$is the velocity vector, $\vec{\sigma} = (0, 0, \sigma)$ is the microrotation, *p*represents pressure, $\vec{g}$stands for gravity and refer nomenclature for all other parameters.

Following are the assumptions made in this problem, which are absolutely arguable:

- The rheological properties of the fluid are constant.
- The fluid motion is in a steady state.
- A porous medium is assumed to have high porosity$(\varepsilon = 1)$.
- No spin boundary condition for microrotation is considered at the isothermal boundary.
- The fluid remains at rest in the infinity position. Hence, fluid velocity is zero at infinity.
- Microstructure impacts are negligible.

The governing Eqs. (1–5) along with the assumptions are reduced to coupled PDEs (Nagaraju et al. [43]. & Aslani et al. [44].):

$$\frac{\partial u}{\partial x} + \frac{\partial \mathrm{v}}{\partial y} = 0, \tag{6}$$

$$u\frac{\partial u}{\partial x}+\mathrm{v}\frac{\partial u}{\partial y}=-\frac{1}{\rho_{tnf}}\frac{\partial p}{\partial x}+\left(\nu_{tnf}+\frac{m}{\rho_{tnf}}\right)\left(\frac{\partial^2 u}{\partial x^2}+\frac{\partial^2 u}{\partial y^2}\right)-\frac{\mu_{tnf}}{\rho_{tnf}k}u+\frac{m}{\rho_{tnf}}\frac{\partial \sigma}{\partial y}, \tag{7}$$

$$u\frac{\partial \mathrm{v}}{\partial x}+\mathrm{v}\frac{\partial \mathrm{v}}{\partial y}=-\frac{1}{\rho_{tnf}}\frac{\partial p}{\partial y}+\left(\nu_{tnf}+\frac{m}{\rho_{tnf}}\right)\left(\frac{\partial^2 \mathrm{v}}{\partial x^2}+\frac{\partial^2 \mathrm{v}}{\partial y^2}\right)-\frac{\mu_{tnf}}{\rho_{tnf}k}\mathrm{v}+\frac{m}{\rho_{tnf}}\frac{\partial \sigma}{\partial x}, \tag{8}$$

$$u\frac{\partial \sigma}{\partial x}+\mathrm{v}\frac{\partial \sigma}{\partial y}=\frac{\gamma}{J\rho_{tnf}}\left(\frac{\partial^2 \sigma}{\partial x^2}+\frac{\partial^2 \sigma}{\partial y^2}\right)-\frac{m}{J\rho_{tnf}}\left(2\sigma+\frac{\partial u}{\partial y}\right)+m\left(\frac{\partial \mathrm{v}}{\partial x}-\frac{\partial u}{\partial y}\right), \tag{9}$$

$$u\frac{\partial T_1}{\partial x}+\mathrm{v}\frac{\partial T_1}{\partial y}=\alpha_{tnf}\left(\frac{\partial^2 T_1}{\partial x^2}+\frac{\partial^2 T_1}{\partial y^2}\right)-\frac{1}{(\rho C_p)_{tnf}}\frac{\partial q_r}{\partial y}, \tag{10}$$

$$u\frac{\partial c}{\partial x}+\mathrm{v}\frac{\partial c}{\partial y}=D\left(\frac{\partial^2 c}{\partial x^2}+\frac{\partial^2 c}{\partial y^2}\right)-K(c-c_\infty). \tag{11}$$

Applying the boundary layer flow assumptions on Eqs. (6–11), we get,

$$\frac{\partial u}{\partial x}+\frac{\partial \mathrm{v}}{\partial y}=0, \tag{12}$$

$$u\frac{\partial u}{\partial x}+\mathrm{v}\frac{\partial u}{\partial y}=\left(\nu_{tnf}+\frac{m}{\rho_{tnf}}\right)\frac{\partial^2 u}{\partial y^2}-\frac{\mu_{tnf}}{\rho_{tnf}k}u+\frac{m}{\rho_{tnf}}\frac{\partial \sigma}{\partial y}, \tag{13}$$

$$u\frac{\partial \sigma}{\partial x}+\mathrm{v}\frac{\partial \sigma}{\partial y}=\frac{\gamma}{J\rho_{tnf}}\frac{\partial^2 \sigma}{\partial y^2}-\frac{m}{J\rho_{tnf}}\left(2\sigma+\frac{\partial u}{\partial y}\right)-m\frac{\partial u}{\partial y}, \tag{14}$$

$$u\frac{\partial T_1}{\partial x}+\mathrm{v}\frac{\partial T_1}{\partial y}=\alpha_{tnf}\frac{\partial^2 T_1}{\partial y^2}-\frac{1}{(\rho C_p)_{tnf}}\frac{\partial q_r}{\partial y}, \tag{15}$$

$$u\frac{\partial c}{\partial x}+\mathrm{v}\frac{\partial c}{\partial y}=D\frac{\partial^2 c}{\partial y^2}-K(c-c_\infty), \tag{16}$$

where *Er*is called Eringen parameter, *J*stands for micro-inertia per unit mass, *K*stands chemical reaction parameter and γ is known as spin gradient viscosity and refer nomenclature for all other parameters.

The following imposed boundary conditions are:

$$\left.\begin{aligned} &u=d\,a\,x+S_1\frac{\partial u}{\partial y}+S_2\frac{\partial^2 u}{\partial y^2},\ \mathrm{v}=\mathrm{v}_w,\ \sigma=-\Gamma\frac{\partial u}{\partial y},\\ &T_1=T_{1_w}+S_3\frac{\partial T_1}{\partial y},\ c=c_w+S_4\frac{\partial c}{\partial y} \end{aligned}\right\}\text{at } y=0 \tag{17}$$

$$u\to 0,\ \sigma\to 0,\ T_1\to T_{1_\infty},\ c\to c_\infty \text{ as } y\to\infty. \tag{18}$$

3. Physical quantities

3.1. The thermal properties of the ternary nanoparticles are as follows [45,46]

- Dynamic viscosity: $\mu_{tnf}=\frac{\phi_1\mu_{nf1}+\phi_2\mu_{nf2}+\phi_3\mu_{nf3}}{\phi}$,
- Density: $\rho_{tnf}=(1-\phi_1-\phi_2-\phi_3)\rho_f+\phi_1\rho_1+\phi_2\rho_2+\phi_3\rho_3$,
- Heat capacity: $(\rho C_p)_{tnf}=(1-\phi_1-\phi_2-\phi_3)(\rho C_p)_f+(\rho C_p)_1\phi_1+(\rho C_p)_2\phi_2+(\rho C_p)_3\phi_3$,
- Kinematic viscosity:$\kappa_{tnf}=\frac{\kappa_{nf1}\phi_1+\kappa_{nf2}\phi_2+\kappa_{nf3}\phi_3}{\phi}$ where,

$$\phi=\phi_1+\phi_2+\phi_3.$$

Density of nanoparticles with spherical shape:

$$\frac{\mu_{nf1}}{\mu_f}=1+2.5\phi+6.2\phi^2,\kappa_{nf1}=\kappa_f\left[\frac{\kappa_1+2\kappa_f-2\phi(\kappa_f-\kappa_1)}{\kappa_1+2\kappa_f+\phi(\kappa_f-\kappa_1)}\right].$$

Density of nanoparticles with cylindrical shape:

$$\frac{\mu_{nf2}}{\mu_f} = 1 + 13.5\phi + 904.4\phi^2, \kappa_{nf2} = \kappa_f \left[\frac{\kappa_2 + 3.9\kappa_f - 3.9\phi(\kappa_f - \kappa_2)}{\kappa_2 + 3.9\kappa_f + (\kappa_f - \kappa_2)\phi}\right].$$

Density of nanoparticles with platelet shape:

$$\frac{\mu_{nf3}}{\mu_f} = 1 + 37.1\phi + 612.6\phi^2, \kappa_{nf3} = \kappa_f \left[\frac{\kappa_3 + 4.7\kappa_f - 4.7\phi(\kappa_f - \kappa_3)}{\kappa_3 + 4.7\kappa_f + \phi(\kappa_f - \kappa_3)}\right].$$

3.2. Radiative heat flux (q_r)

The investigator Rosseland [50] approximated the radiative heat flux as $q_r = -\frac{4\sigma^*}{3k^*}\frac{\partial T_1^4}{\partial y}$, where $\sigma^*$is known as SB constant and $k^*$is known as absorption coefficient. In this investigation, it is assumed that T_1^4can be expressed in the form of series about the point T_{1_∞}using Taylor series expansion of second order. This assumption is due to the temperature variation in the flow. Therefore, T_1^4 is approximated as:$T_1^4 \cong 4T_{1_\infty}^3 T_1 - 3T_{1_\infty}^4$. Using this approximation, we get

$$q_r = -\frac{16\sigma^* T_{1_\infty}^3}{3k^*}\frac{\partial T_1}{\partial y} \text{ and } \frac{\partial q_r}{\partial y} = -\frac{16\sigma^* T_{1_\infty}^3}{3k^*}\frac{\partial^2 T_1}{\partial y^2}. \tag{20}$$

Now, Eq. (15) is reduced to the following equation.

$$u\frac{\partial T_1}{\partial x} + v\frac{\partial T_1}{\partial y} = \alpha_{tnf}\frac{\partial^2 T_1}{\partial y^2} + \frac{16\sigma^* T_{1_\infty}^3}{3k^*(\rho C_p)_{tnf}}\frac{\partial^2 T_1}{\partial y^2}. \tag{21}$$

3.3. Spin gradient viscosity

In order to achieve the high performance in the fluid flow, the spin gradient viscosity [51] is modeled as below so that the microrotation is turned down to angular velocity and the microstructure effects are neglected.

$$\gamma = \left(\mu_{tnf} + \frac{m}{2}\right)J \quad \text{where} \quad J = \frac{\nu_{tnf}}{a}. \tag{22}$$

4. Solution interpretation

The governing Eqs. (12–16) are reduced to ODEs and solved analytically using the below listed non-dimensional variables. With radiation and chemical reactive fluid along with slip effects, the energy and concentration equations are solved by analytical technique and expressed in terms of incomplete gamma functions by introducing new variables. Applying the assumptions made earlier in this investigation, the pressure gradient and the external forces are ignored. Also, the distance between the slip and the stretching/shrinking sheet is linear.

$$X = \left(\frac{a}{\nu}\right)^{1/2} x, Y = \left(\frac{a}{\nu}\right)^{1/2} y, N = \frac{\sigma}{a}, (U, V) = \frac{(u, v)}{(a\nu)^{1/2}}, T_2 = \frac{T_1 - T_{1_\infty}}{T_{1_w} - T_{1_\infty}} \text{ and } C = \frac{C - C_\infty}{C_w - C_\infty}. \tag{23}$$

Therefore, Eqs. (12–14), (16) & (21) are reduced to non-dimensional equations using Eq. (23).

$$\frac{\partial U}{\partial X} + \frac{\partial U}{\partial Y} = 0, \tag{24}$$

$$U\frac{\partial U}{\partial X} + V\frac{\partial U}{\partial Y} = \left(\nu_{tnf} + \frac{m}{\rho_{tnf}}\right)\frac{\partial^2 U}{\partial Y^2} - \frac{\mu_{tnf}}{\rho_{tnf} k}U + \frac{m}{\rho_{tnf}}\frac{\partial N}{\partial Y}, \tag{25}$$

$$U\frac{\partial N}{\partial X} + V\frac{\partial N}{\partial Y} = \left(1 + \frac{m}{2\mu_{tnf}}\right)\frac{\partial^2 N}{\partial Y^2} - \frac{m}{\mu_{tnf}}\left(2N + \frac{\partial U}{\partial Y}\right), \tag{26}$$

$$U\frac{\partial T_2}{\partial x} + V\frac{\partial T_2}{\partial y} = \frac{\alpha_{tnf}}{\nu_{bf}}\frac{\partial^2 T_2}{\partial Y^2} + \frac{16\sigma^* T_{2_\infty}^3}{3k^*(\rho C_p)_{tnf}\nu}\frac{\partial^2 T_2}{\partial Y^2}, \tag{27}$$

$$U\frac{\partial C}{\partial X} + V\frac{\partial C}{\partial Y} = \frac{D}{\nu_{bf}}\frac{\partial^2 C}{\partial Y^2} - \frac{K}{\nu_{bf}}C, \tag{28}$$

the associated boundary conditions are:

$$\left.\begin{aligned} &U = dX + S_1\sqrt{\frac{a}{\nu}}\frac{\partial U}{\partial Y} + S_2\sqrt{\frac{a}{\nu}}\frac{\partial^2 U}{\partial Y^2}, V = V_w, N = -\Gamma\frac{\partial U}{\partial Y} \\ &T_2 = 1 + S_3\sqrt{\frac{a}{\nu}}\frac{\partial T_2}{\partial Y} \text{ and } C = 1 + S_4\sqrt{\frac{a}{\nu}}\frac{\partial C}{\partial Y} \end{aligned}\right\} \text{at } Y = 0 \tag{29}$$

$$U = 0,\ N = 0,\ T_2 \to T_{2_\infty} \text{ and } C \to C_\infty \text{ as } Y = \infty \tag{30}$$

5. Similarity transformations

In this study, the governing PDEs are simplified, resulting in an ODEs system via a series of typical similarity transformations. These changes are described as:

The stream function is $\Psi(X, Y) = XF(Y)$and the similarity variables are given by,

$$U = \frac{\partial \Psi}{\partial Y}, \quad V = -\frac{\partial \Psi}{\partial X}, \quad N = XG(Y), \quad T_2 = \Theta(Y) \text{ and } C = \Phi(Y). \tag{31}$$

Using the above transformations, the continuity equation is satisfied, while Eqs.(25)–(28) are reduced to the following ODEs:

$$\left(1 + \frac{ErA_3}{A_1}\right)\frac{d^3F}{dY^3} + F\frac{d^2F}{dY^2} - \left(\frac{A_1(Da)^{-1}}{A_2}\right)\frac{dF}{dY} - \left(\frac{dF}{dY}\right)^2 + \left(\frac{ErA_3}{A_1}\right)\frac{dG}{dY} = 0, \tag{32}$$

$$\left(1 + \frac{ErA_3}{2A_1}\right)\frac{d^2G}{dY^2} + F\frac{dG}{dY} - \left(\frac{ErA_3}{A_1}\right)\left(2G + \frac{d^2F}{dY^2}\right) - G\frac{dF}{dY} = 0, \tag{33}$$

$$(A_3 + N_r)\frac{d^2\Theta}{dY^2} + PrA_4F\frac{d\Theta}{dY} = 0, \tag{34}$$

$$\frac{d^2\Phi}{dY^2} + ScF\frac{d\Phi}{dY} - K_1Sc\Phi = 0. \tag{35}$$

The resultant boundary conditions are as follows:

$$\left.\begin{aligned} &F(0) = V_c, \quad \frac{dF(0)}{dY} = d + \lambda_1\frac{d^2F(0)}{dY^2} + \lambda_2\frac{d^3F(0)}{dY^3}, \quad G(0) = -\Gamma\frac{d^2F(0)}{dY^2}, \\ &\Theta(0) = 1 + \lambda_3\frac{d\Theta(0)}{dY} \quad \text{and} \quad \Phi(0) = 1 + \lambda_4\frac{d\Phi(0)}{dY}. \end{aligned}\right\} \tag{36}$$

$$\frac{dF(\infty)}{dY} = 0, G(\infty) = 0, \Theta(\infty) = 0 \text{ and } \Phi(\infty) = 0. \tag{37}$$

Here,

$$Er = \frac{\kappa_f}{\mu_f}, (Da)^{-1} = \frac{\nu_f}{a\kappa_f}, N_r = \frac{16\sigma^* T^3_{2_\infty}}{3k^*\kappa_f}, K_1 = \frac{K}{\nu_f}, \Pr = \frac{\nu_f}{\alpha_f}, Sc = \frac{\nu_f}{D}, \tag{38}$$

$$V_c = -\frac{v_w}{\sqrt{a\nu}}, \quad \lambda_1 = S_1\sqrt{\frac{a}{\nu}}, \quad \lambda_2 = S_2\sqrt{\frac{a}{\nu}}, \quad \lambda_3 = S_3\sqrt{\frac{a}{\nu}} \quad \text{and} \quad \lambda_4 = S_4\sqrt{\frac{a}{\nu}}. \tag{39}$$

Further,

$$A_1 = \frac{\phi_1B_1 + \phi_2B_2 + \phi_3B_3}{\phi}, A_2 = 1 - \phi_1 - \phi_2 - \phi_3 + \phi_1\frac{\rho_{sp1}}{\rho_f} + \phi_2\frac{\rho_{sp2}}{\rho_f} + \phi_3\frac{\rho_{sp3}}{\rho_f}$$

$$A_3 = \frac{\phi_1B_4 + \phi_2B_5 + \phi_3B_6}{\phi}, A_4 = 1 - \phi_1 - \phi_2 - \phi_3 + \phi_1\frac{(\rho c_p)_{sp1}}{(\rho c_p)_f} + \phi_2\frac{(\rho c_p)_{sp2}}{(\rho c_p)_f} + \phi_3\frac{(\rho c_p)_{sp3}}{(\rho c_p)_f}$$

$$B_1 = 1 + 2.5\phi + 6.2\phi^2, B_2 = 1 + 13.5\phi + 904.4\phi^2, B_3 = 1 + 37.1\phi + 612.6\phi^2, B_4 = \left[\frac{\kappa_{sp1} + 2\kappa_f - 2\phi(\kappa_f - \kappa_{sp1})}{\kappa_{sp1} + 2\kappa_f + \phi(\kappa_f - \kappa_{sp1})}\right], B_5 = \left[\frac{\kappa_{sp2} + 3.9\kappa_f - 3.9\phi(\kappa_f - \kappa_{sp2})}{\kappa_{sp2} + 3.9\kappa_f + \phi(\kappa_f - \kappa_{sp2})}\right]$$

and

$$B_6 = \left[\frac{\kappa_{sp3} + 4.7\kappa_f - 4.7\phi(\kappa_f - \kappa_{sp3})}{\kappa_{sp3} + 4.7\kappa_f + \phi(\kappa_f - \kappa_{sp3})}\right].$$

6. Analytical solution for velocity and microrotation

Earlier works by Turkyilmazoglu [52], Crane [53], Aslani et al. [54]. and Nagaraj et al. [55]. explain the solutions of velocity and microrotation equations. The analytical solutions to Eqs. (32)and (33) corresponding to the boundary conditions Eqs. (36) and (37) are obtained as follows:

$$F(Y) = V_c + \frac{d[1 - Exp(-\beta Y)]}{\beta(1 + \lambda_1\beta - \lambda_2\beta^2)} \quad \text{and} \quad G(Y) = -\Gamma\frac{d^2F}{dY^2} \tag{40}$$

Now, we obtain the algebraic equation as below by substituting Eq. (39) in Eqs. (32) and Eq. (33).

$$p_1\beta^4 + q_1\beta^3 + r_1\beta^2 - s_1\beta - t_1 = 0 \tag{41}$$

where,

$$p_1 = -\left(1 + \frac{Er A_3}{A_1}\right)\lambda_2, q_1 = \left(1 + \frac{Er A_3}{A_1}\right)\lambda_1 + V_c\lambda_2, s_1 = \left(\frac{A_1(Da)^{-1}\lambda_1}{A_2} + V_c\right), r_1 = \left(1 + \frac{Er A_3}{A_1}\right) - V_c\lambda_1 + \frac{A_1(Da)^{-1}\lambda_2}{A_2} - \frac{\Gamma Er A_3}{A_1} \text{and } t_1 = \frac{A_1(Da)^{-1}}{A_2} + d.$$

Also,

$$p_{2\beta}^4 - q_{2\beta}^3 - r_{2\beta}^2 + s_{2\beta} + t_2 = 0 \tag{42}$$

where,

$$p_2 = \left(1 + \frac{ErA_3}{2A_1}\right)\Gamma\lambda_2, \quad q_2 = \left[\left(1 + \frac{ErA_3}{2A_1}\right)\Gamma\lambda_1 + \Gamma\lambda_2 V_c - \left(\frac{ErA_3}{A_1}\right)\lambda_2\right], \}$$

$$r_2 = \left[\left(1 + \frac{ErA_3}{2A_1}\right)\Gamma - \Gamma V_c\lambda_1 + (2\Gamma\lambda_2 + \lambda_1)\left(\frac{ErA_3}{A_1}\right)\right],$$

$$s_2 = \left[\Gamma V_c + (2\Gamma\lambda_2 + 1)\left(\frac{ErA_3}{A_1}\right)\right], \; t_2 = \left[d + 2\left(\frac{ErA_3}{A_1}\right)\right]\Gamma.$$

Here Γis the parameter constant which lies between 0 and 1. In this investigation, analytical solution is obtained by considering $\Gamma = \frac{1}{2}$(refers to weak concentration of micro-particles). While, $\Gamma = 0$ represents a strong concentration of micro-particles and $\Gamma = 1$represents turbulent flow of the fluid.

Solving the algebraic equation in Eq. (40) we obtain four real roots as below:

$$\beta_{1,2} = -\frac{q_1}{4p_1} - \frac{1}{2}\sqrt{\frac{q_1^2}{4p_1^2} - \frac{2r_1}{3p_1} + \frac{\delta_1}{3p_1(\delta_2)^{1/3}} + \frac{(\delta_2)^{1/3}}{3(2)^{1/3}p_1}} \mp \frac{1}{2}\sqrt{\frac{q_1^2}{2p_1^2} - \frac{4r_1}{3p_1} + \frac{\delta_1}{3p_1(\delta_2)^{1/3}} - \frac{\delta_2}{3(2)^{1/3}p_1}} - \frac{\frac{8s_1}{p_1} + \frac{4q_1r_1}{p_1^2} - \frac{q_1^3}{p_1^3}}{\sqrt{\frac{q_1^2}{4p_1^2} - \frac{2r_1}{3p_1} + \frac{\delta_1}{3p_1(\delta_2)^{1/3}} + \frac{(\delta_2)^{1/3}}{3(2)^{1/3}p_1}}},$$

$$\beta_{3,4} = -\frac{q_1}{4p_1} + \frac{1}{2}\sqrt{\frac{q_1^2}{4p_1^2} - \frac{2r_1}{3p_1} + \frac{\delta_1}{3p_1(\delta_2)^{1/3}} + \frac{(\delta_2)^{1/3}}{3(2)^{1/3}p_1}} \mp \frac{1}{2}\sqrt{\frac{q_1^2}{2p_1^2} - \frac{4r_1}{3p_1} + \frac{\delta_1}{3p_1(\delta_2)^{1/3}} - \frac{\delta_2}{3(2)^{1/3}p_1}} + \frac{\frac{8s_1}{p_1} + \frac{4q_1r_1}{p_1^2} - \frac{q_1^3}{p_1^3}}{\sqrt{\frac{q_1^2}{4p_1^2} - \frac{2r_1}{3p_1} + \frac{\delta_1}{3p_1(\delta_2)^{1/3}} + \frac{(\delta_2)^{1/3}}{3(2)^{1/3}p_1}}},$$

with, $\delta_1 = (2)^{1/3}(r^2 + 3qs - 12pt)$ and
$\delta_2 = 2r^3 + 9qrs + 27ps^2 - 27q^2t + 72prt + \sqrt{-4(r^2 + 3qs - 12pt)^3 + (2r^3 + 9qrs + 27ps^2 - 27q^2t + 72prt)^2}.$

6.1. Temperature analysis

The temperature equation in Eq. (34) is reduced to find the solution in terms of an incomplete gamma function by setting a new variable $\zeta = \left(\frac{d\mathrm{Pr}}{\beta^2}\right)e^{-\beta Y}$ and substituting in Eq. (34), we get the following differential equation:

$$\zeta\,\Theta_{\zeta\zeta} + (1 - l + m\zeta)\Theta_{\zeta} = 0, \tag{43}$$

Along with the corresponding boundary conditions

$$\Theta\left(\zeta = \frac{d\mathrm{Pr}}{\beta^2}\right) = 1 + \lambda_3\Theta_{\zeta}\left(\zeta = \frac{d\mathrm{Pr}}{\beta^2}\right) \quad \text{and} \quad \Theta(\zeta = 0) \tag{44}$$

by considering,

$$l = \frac{V_c A_4 \mathrm{Pr}}{\beta(A_3 + R)} + \frac{\varsigma A_4 \mathrm{Pr}}{\beta^2\left(1 + \lambda_1\beta - \lambda_2\beta^2\right)(A_3 + R)} \text{ and } m = \frac{A_4}{(A_3 + R)\left(1 + \lambda_1\beta - \lambda_2\beta^2\right)}. \tag{45}$$

Upon solving Eq. (42) using the boundary conditions as in Eq. (43), we get an analytical solution for the temperature equation.

$$\Theta(Y) = \frac{\Gamma[l, 0] - \Gamma\left[l, \frac{md\mathrm{Pr}}{\beta^2}e^{-\beta Y}\right]}{\lambda_3\beta m^l\left(\frac{d\mathrm{Pr}}{\beta^2}\right)^l e^{-\frac{md\mathrm{Pr}}{\beta^2}} + (1 - \lambda_3)\Gamma[l, 0] - \Gamma\left[l, \frac{md\mathrm{Pr}}{\beta^2}\right]}. \tag{46}$$

7. Concentration analysis

The solution of the concentration Eq. (35) is explored by the substituting $F(Y)$ and also by framing a new variable as $\chi = \left(\frac{d\,Sc}{\beta^2}\right)e^{-\beta Y}$, such that Eq. (35) is reduced to the following:

$$\chi\,\frac{d^2\Phi}{d\chi^2} + (1 - a + b\chi)\frac{d\Phi}{d\chi} - \frac{K_1 Sc}{\beta^2\chi}\Phi = 0, \tag{47}$$

which is associated with boundary conditions

$$\Phi(\chi = 0) = 0 \quad \text{and} \quad \Phi\left(\chi = \frac{d\,Sc}{\beta^2}\right) = 1 + \lambda_4\,\frac{d\Phi}{dY}\left(\chi = \frac{d\,Sc}{\beta^2}\right). \tag{48}$$

Here,

$$a = \frac{Sc\;V_c}{\beta} + \frac{Sc\,d}{\beta^2\left(1 + \lambda_1\beta - \lambda_2\beta^2\right)} \quad \text{and} \quad b = \frac{1}{\left(1 + \lambda_1\beta - \lambda_2\beta^2\right)}. \tag{49}$$

Eq. (46) is solved using Eq. (47) and the solution is represented in terms of Hypergeometric functions:

$$\Phi(Y) = \frac{\left[\frac{d\,Sc\,e^{-\beta Y}}{\beta^2}\right]^{\frac{w_1+w_2}{2}}{}_1F_1\left[w_1 + w_2,\; w_2 + 1,\; \left(\frac{b\,d\,Sc\,e^{-\beta Y}}{\beta^2}\right)\right]}{\left(\frac{d\,Sc}{\beta^2}\right)^{\frac{w_1+w_2}{2}}\left\{\begin{array}{l}\left[1 - \lambda_4\left(\frac{w_1 + w_2}{2}\right)\left(\frac{\beta^2}{d\,Sc}\right)\right]{}_1F_1\left[w_1 + w_2,\; w_2 + 1,\; \left(\frac{b\,d\,Sc}{\beta^2}\right)\right] + \\ \beta\,b\left(\frac{d\,Sc\,e^{-\beta Y}}{\beta^2}\right){}_1F_1\left[w_1 + w_2 + 1,\; w_2 + 2,\; \frac{b\,d\,Sc}{\beta^2}\right]\end{array}\right\}}. \tag{50}$$

where, w_1 and w_2 are constants.

Hence Eq. (49) serves as a solution for the concentration equation.

8. Parameters of physical interest

The dimensionless factor of skin friction is defined as follows:

$$\sqrt{\mathrm{Re}}\,C_{fx} = \left[\frac{A_1 + (1 - \Gamma)\,Er\,A_3}{A_2}\right]\left(\frac{d^2F}{dY^2}\right)_{Y=0}, \tag{51}$$

where,

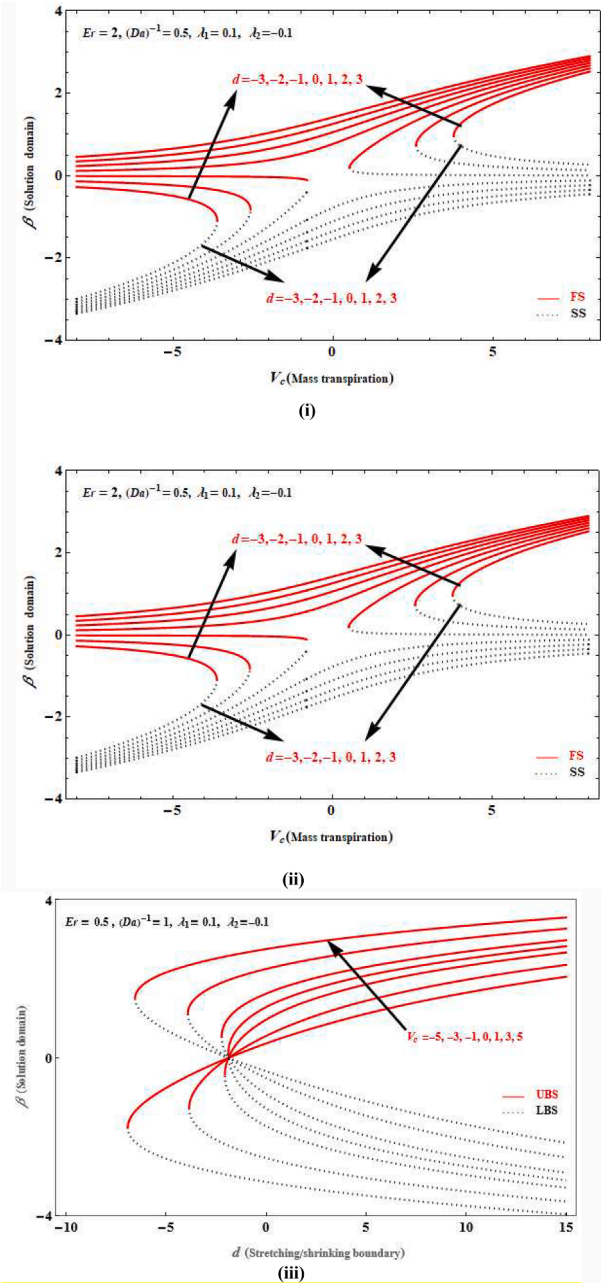

Fig. 2. (i)-(iii): Domain demonstrating the solution for the controlling parameters.

$$C_{f\,x} = \frac{\left[\left(\mu_{tnf} + m\right)\left(\frac{\partial u}{\partial y}\right) + \frac{\kappa_{tnf}}{a} N\right]_{y=0}}{\rho_{tnf}\, u_w^2}, \tag{52}$$

and,

$\mathrm{Re}_x = \frac{a\,x^2}{\nu_f}$ is known as Reynolds number.

Nusselt number is defined as,

$$Nu_x Re^{-1/2} = -(A_3 + N_r)\theta'(0) \tag{53}$$

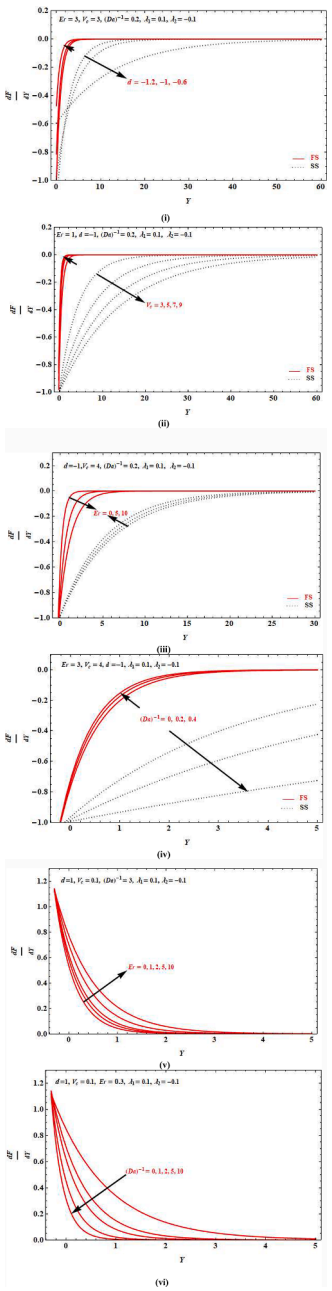

Fig. 3. (i)-(vi): Solution plot of the axial velocity for the various physical parameters.

$$Nu_x = -\frac{x\left(\kappa_{tnf} + \frac{16\sigma^* T_\infty^3}{3k^*}\right)\frac{\partial T}{\partial y}\Big|_{y=0}}{\kappa_f (T_w - T_\infty)}. \tag{54}$$

9. Outcomes of the investigation

The current work examines the MPF flow via a shrinking/stretching surface that is sensitive to internal radiation, chemical reaction, and mass transpiration and multiple slip conditions. By resolving the collection of ODEs, analytical solutions are expressed as an incomplete gamma function for the energy equation and a confluent hypergeometric function for the mass equation. For different dimensionless parameter values of the flow, including the stretching/shrinking parameter d,inverse of Darcy number$(Da)^{-1}$, Prandtl number Pr, Eringen parameterEr, Schmidt number Sc, slip parameters$\lambda_1/\lambda_2/\lambda_3/\lambda_4$, chemical reaction parameter $K_1$and radiation

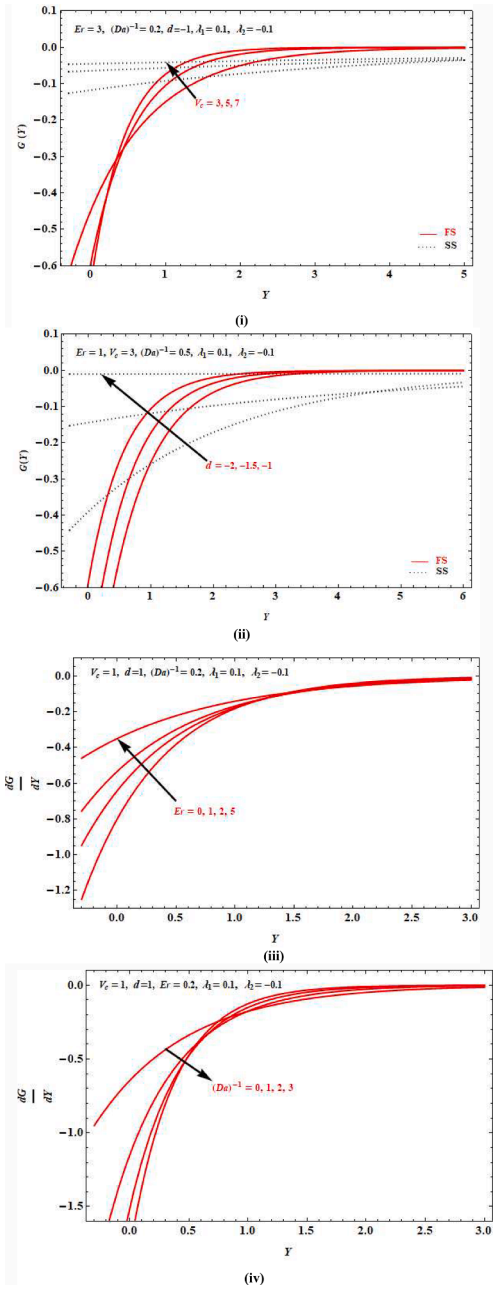

Fig. 4. (a)-(d): Solution plot of the transverse and axial velocities for the various physical parameters.

parameter R plots of $\frac{dF}{d\eta}$, $G(\eta)$, $\frac{dG}{d\eta}$, $\Theta(\eta)$ and $\Phi(\eta)$are obtained and discussed below. The numbers $\beta$and $\Gamma$are also two more essential parameters in this study. The solution of the governing equations contains both parameters (refer Section 6). Note, the value of $\Gamma = \frac{1}{2}$is considered, which causes anti-symmetric portion of the stress tensor to vanish, which results low concentration of micro-components [56]. This mandates that only Eq. (40) can be used to calculate (see again Sect. 6). The FS and SS for the value ofβ are determined from this equation. There are several studies that examine the physical significance of the multiple solutions within this framework. The energy transfer of nanofluid flow over a shrinking/stretching surface was examined by Zaimi et al. [57]. and Merkin [58]. They came to the conclusion that the first solution, which was backed by their findings, was the physically feasible solution. Additionally, SS resulted in infinite boundary conditions in the case of velocity for a set of parameter values; as a result, this solution may be automatically discarded.

The domain of the solution with respect to$V_c$which is a function of$Er$and$d$, is represented in Figs. 2(a) and 2(b) respectively. Also, the domain of the solution with respect to$d$which it is a function of V_c is shown in Fig. 2(c). While decreasing the SS, increasing

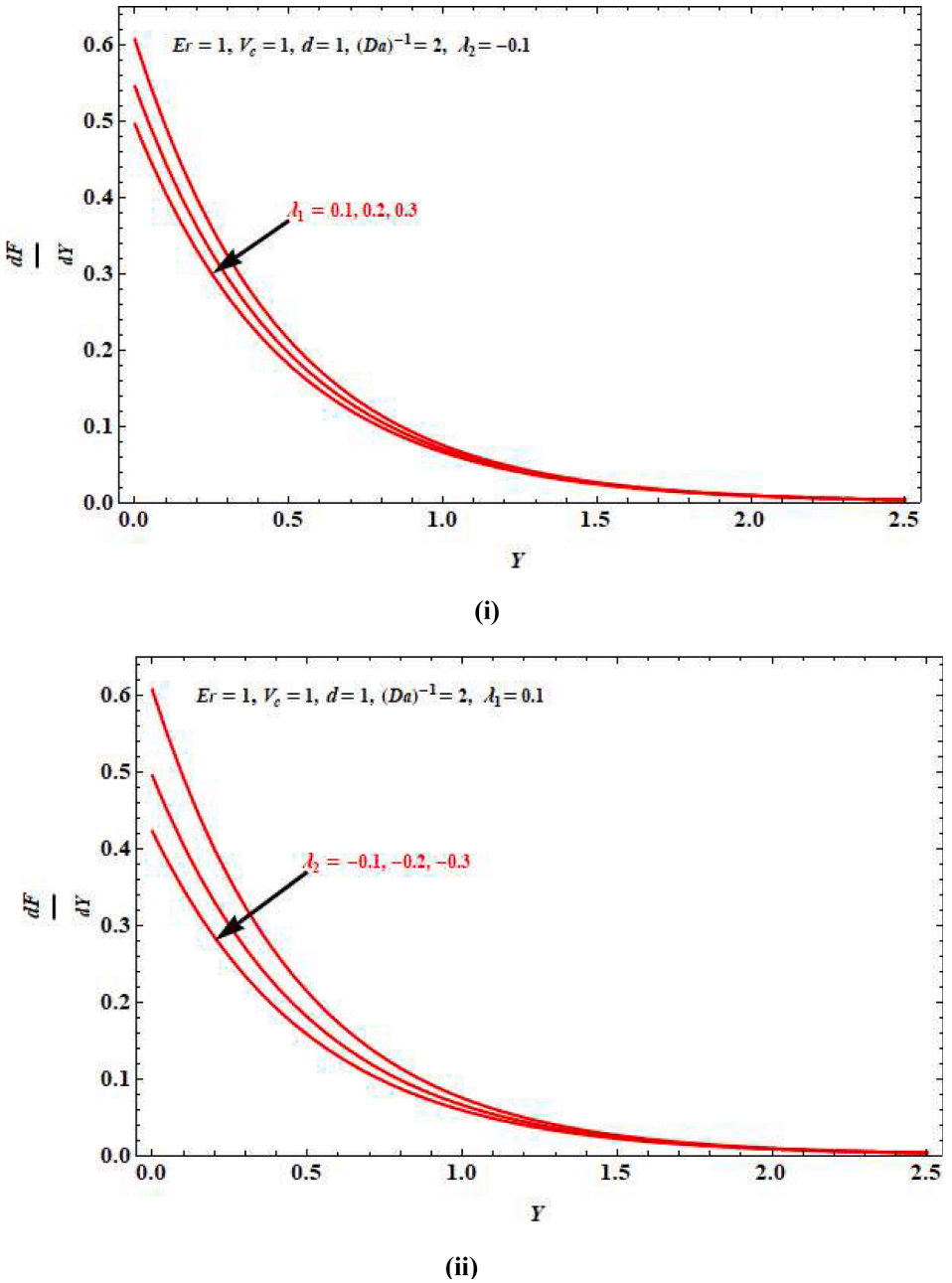

Fig. 5. (i)-(ii): Axial velocity plot for the slip parameters.

parameter d increases the FS. The SS is increased while the FS is decreased as the parameters Er and $V_c$are increased. Fig. 2 makes it clear that it is highly dependent on the variablesV_c, Er, and d.

Fig. 3(i)–3(iv) show the impacts of the $d \leq -1$, $V_c > 0$, Er, and $(Da)^{-1}$for the shrinking case for constant values of the parameters on the velocity of the flow. When the $d \leq -1$, all of the sheet's pulling force is physically transferred to the fluid, as shown in Fig. 3(i), which examines the influence of shrinking parameter on velocity. When comparing the axial velocities of the FS and SS, it is obvious that the top branch's axial velocities exhibit an angled gradient towards the boundary, which indicates a potential cause for more shear stress on the boundary. The force acting on the sheet boundary's decrease could also be understood as increased shear stress. As seen in Fig. 3(i), flow velocity increases in the FS and drops in the SS as the shrinking parameter is increased. As shown in Fig. 3(ii) and Fig. 3 (iv), similar impacts were seen for the $V_c > 0$ and $(Da)^{-1}$.In contrast, flow velocity improved as the Er decreased for the FS and declines for the SS in the case of the Er (see Fig. 3(iii)).

In the case of the stretching sheet, the axial velocity profiles are shown in Fig. 3(v) and 3(vi) for various values of the Er and $(Da)^{-1}$.

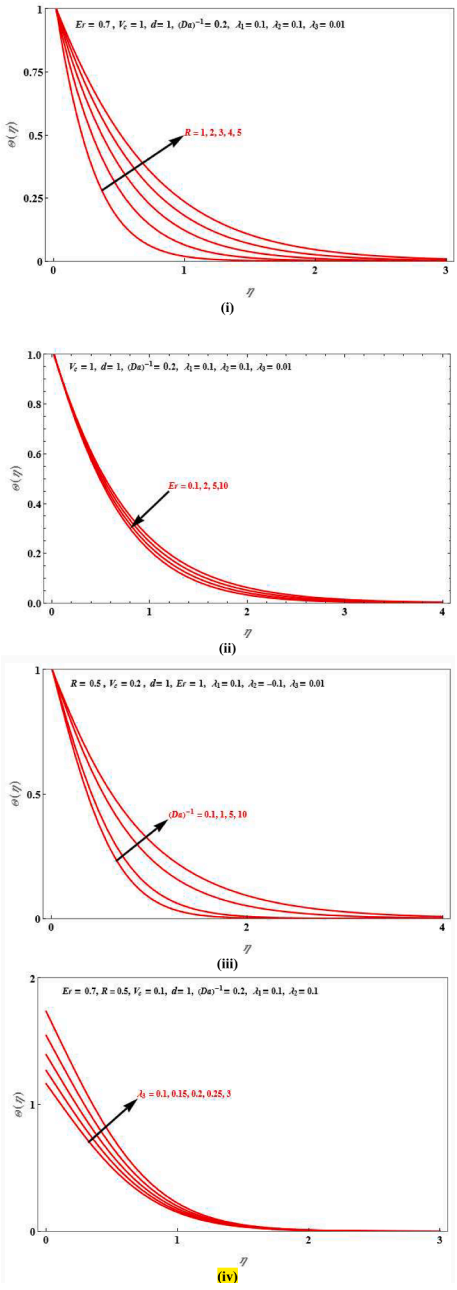

Fig. 6. (i)-(iv): Thermal profile plots for various parameters.

Due to the presence of non-Newtonian fluid, additional force, microrotation is created along with viscous force, an increase in the *Er* value, increases the flow velocity, which means that, the boundary layer is more thickened with the increase in the *Er*. As can be seen from Fig. 3(vi), the inverse behavior appeared in the case of the $(Da)^{-1}$. As a result, in every instance, the FS and SS displayed opposing characteristics.

The impacts of $V_c > 0$and $d \leq -1$on the microrotation profiles for both the FS and SS are depicted in Fig. 4(i) and 4(ii). As observed, it is obvious that as the values of V_c and d rise, the velocity due to microrotation in the FS raises while the microrotation in the SS drops. Graphs of the gradient of the microrotation against the variable Y for different *Er* and $(Da)^{-1}$values for the case of $d = 1$are shown in Figs. 4(iii) and 4(iv). While $(Da)^{-1}$ increases, $\frac{dG}{dY}$drops, while *Er* increases and $\frac{dG}{dY}$ follows the same nature. As a result, *Er* and $(Da)^{-1}$ behaves in the opposite trend.

Fig. 5 depicts the effect of slip parameters on the axial velocity of the fluid. It is observed that increased values of Navier's slip

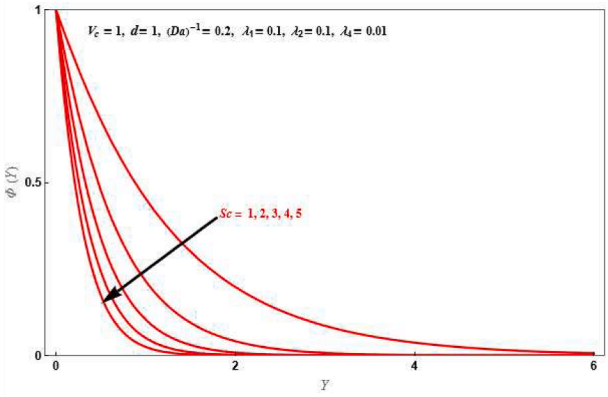

(i)

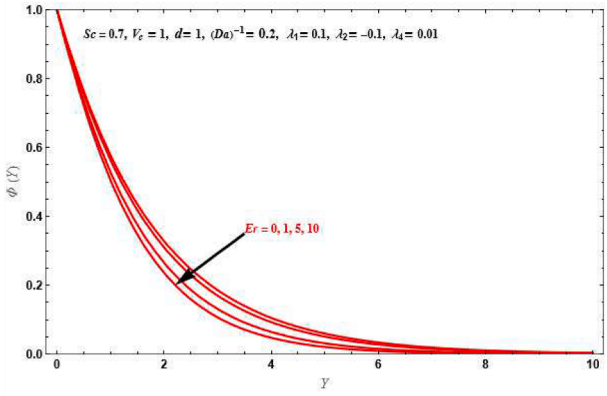

(ii)

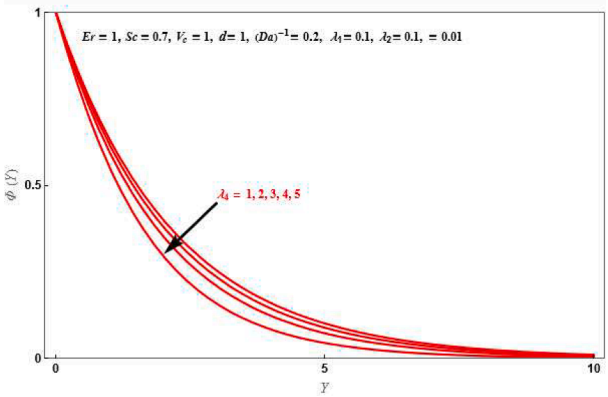

(iii)

Fig. 7. (i)-(iii): Concentration plot for various parameters.

parameter, decrease the velocity of the fluid, while decreasing values of the second order slip parameter decrease the velocity of the fluid.

The radiation parameter R is one of the most significant dimensionless heat transfer characteristics. Fig. 6(i) illustrates the impact of R on the energy profile. It is noted that energy flow is increasing with increasing R value. A similar trend is observed when the $(Da)^{-1}$and $\lambda_3$is increased as shown in Fig. 6(c) and Fig. 6(d). *Er* parameter is affecting the energy of the fluid as shown in Fig. 6(b). As observed, the energy is decreased with the increased value of *Er*.

Plots in Fig. 7(i)-(iii) depicts the significance of the controlling parameters like *Er, Sc* and λ_4.

Plots reveal that increasing values of these parameters *Er, Sc* and $\lambda_4$is decreasing the concentration of the flow.

It is well known that skin friction is influenced by the hydrodynamic boundary layer's thickness. In Fig. 8, the skin friction results

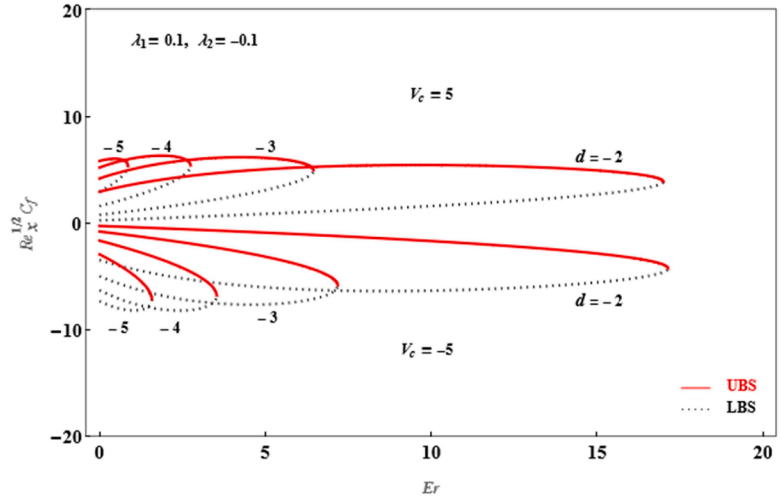

(i)

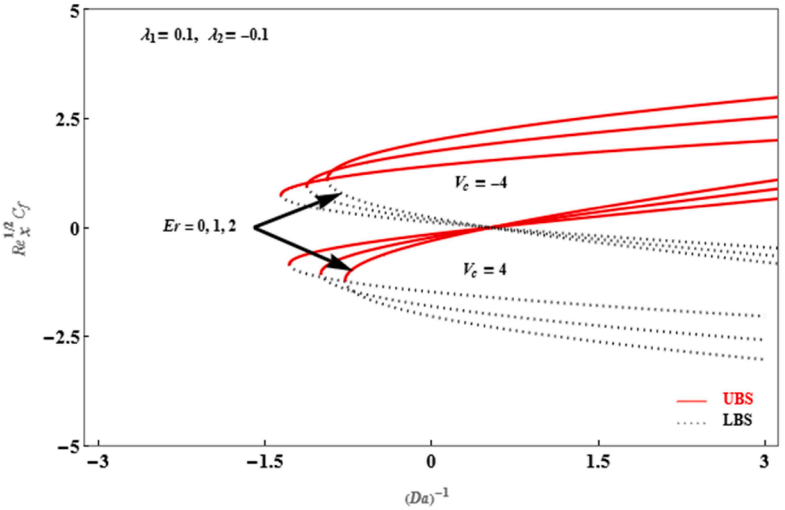

(ii)

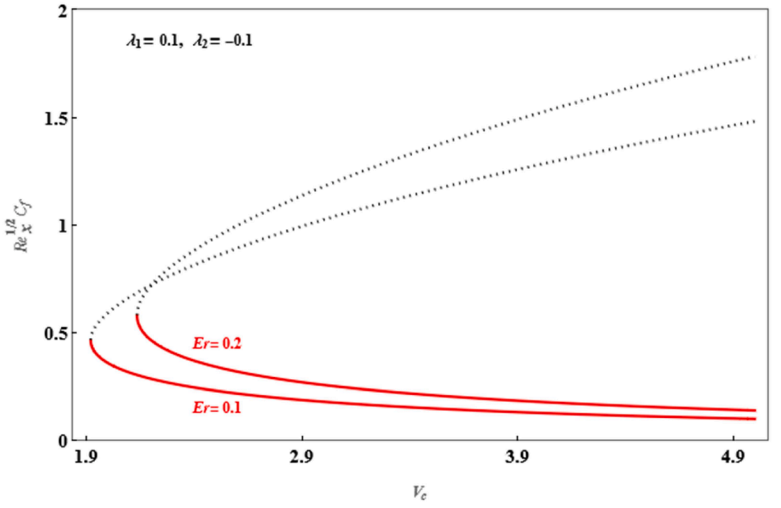

(iii)

(caption on next page)

Fig. 8. (i)-(iii): Skin friction coefficient plot for various parameters.

Table 1
Thermo-physical properties [47–49].

Sl. No.	Fluid Type	C_p	ρ	κ	Shape
1	Water H_2O	4180	997.1	0.613	–
2	Graphene	790	2200	5000	Platelet
3	Copper Oxide (CuO)	765	6320	40	Spherical
4	Single wall CNT	531.8	2600	76.5	Cylindrical

for the shrinking sheet scenario are plotted against Er, $(Da)^{-1}$ and V_c. Skin friction is a complex phenomenon that depends on a number of governing factors, like micropolar fluid flow in porous media, in which the boundary will act as the cause of motion. Fig. 8(i) demonstrates how skin friction rises in proportion to the intensity of boundary motion. However, the valid Er region shrinks due to the stronger shrinkage of the decreasing sheet. It's also crucial to remember that, despite the fact that the FS and SS always exhibit contradictory cases, the associated graphs are identified as non-symmetric on the plane transient from the highest value. Furthermore, the impact of the porous media in the fluid flow direction is represented by the $(Da)^{-1}$. Skin friction is therefore expected to increase when it increases, as seen in Fig. 8(ii).

In addition, as observed in Fig. 8(iii), the smaller Er values will result in slower perspiration on the wall and higher Er values yield greater skin friction between the wall and fluid. When the velocity continuously increasing, the difference between $Er = 0.1$ and $Er = 0.2$ progressively disappears. This is because the fluid micropolarity's effect will be overpowered by the effect of hydrodynamic of the wall infusing (Table 1).

10. Concluding remarks

The flow of the micropolar fluid suspended with ternary nanoparticles over a permeable stretching/shrinking surface that is sensitive to internal radiation, chemical reaction, and mass transpiration and multiple slip conditions is investigated. Analytical solutions are obtained in terms of incomplete gamma functions and confluent hypergeometric functions for the governing differential equations. The following conclusions are listed below based on the results obtained in the investigation.

- Solution domains help in identifying the possible parametric values.
- The existence of multiple solutions for the shrinking case is observed while a unique solution is observed for stretching case.
- The velocity of the tri-hybrid nanofluid is found to increase for the FS and decrease for the SS with increased values of $(Da)^{-1}$, d, and V_c but reverse trend is observed with an increased value of Er.
- Increased values of Navier's and second order slip parameters, decrease the velocity of the flow.
- The impact of R shows greater significance on the temperature profile by increasing the thermal boundary.
- Concentration decreases with increasing value of Er, Sc and λ_4

Declaration of competing interest

The authors declare that they have no known competing financial interests or personal relationships that could have appeared to influence the work reported in this paper.

Acknowledgments

L.M.P. acknowledges partial financial support from ANID through Convocatoria Nacional Subvención a Instalación en la Academia Convocatoria Año 2021, Grant SA77210040.

References

[1] J. Chen, C. Liang, J.D. Lee, Theory and simulation of micropolar fluid dynamics, J. Nanoeng. Nanosyst. 224 (2011) 31–39, https://doi.org/10.1177/1740349911400132.
[2] Hoyt J.W., Fabula A.G.: The effects of additives on fluid friction. US Naval ordinance test station report (1964). https://api.semanticscholar.org/CorpusID:137533644.
[3] W.A. Vogel, A.M. Patterson, An experimental investigation of additives injected into the boundary layer of an underwater body, Pacific Naval Lab. Defense Res. (1964), https://doi.org/10.1007/BF01176097. Board of Canada, Report.
[4] A.C. Eringen, Theory of Micropolar Fluids, J. Math. Anal. Appl. 16 (1966) 1–18, https://doi.org/10.1512/IUMJ.1967.16.16001.
[5] A.C. Eringen, Theory of Thermo-Microfluids, J. Math. Anal. Appl. 38 (1972) 480–496, https://doi.org/10.1016/0022-247X(72)90106-0.
[6] G. Ahmadi, Self-similar solution of incompressible Micropolar boundary layer flow over a semi-infinite plate, Int. J. Eng. Sci. 14 (1976) 639–646, https://doi.org/10.1016/0020-7225(76)90006-9.
[7] T. Hayat, M. Mustafa, S. Obaidat, Soret and dufour effects on the stagnation point flow of a Micropolar fluid toward a stretching sheet, J. Fluid Eng. 133 (2011) 1–9, https://doi.org/10.1115/1.4003505.

[8] M.M. Rahman, Convective flows of Micropolar fluids from radiate isothermal porous surface with viscous dissipation and joule heating, Commun. Nonlinear Sci. Numer. Simul. 14 (2009) 3018–3030, https://doi.org/10.1016/j.cnsns.2008.11.010.

[9] G. Lukaszewicz, Micropolar Fluids: Theory and Applications, Birkhauser, Boston, 1999. https://link.springer.com/book/10.1007/978-1-4612-0641-5.

[10] S. Maryam, U. Naeem, S. Nadeem, A. Arsalan, S. Humara, Modeling and numerical analysis of micropolar hybrid-nanofluid flow subject to entropy generation, Int. J. Mod. Phys. B (2023), https://doi.org/10.1142/S0217979224502850.

[11] S. Nadeem, N. Abbas, A. Saleem, A. Amin, F.M. Alharbi, A. Hussain, A. Issakhoy, Effects of heat and mass transfer on stagnation point flow of micropolar Maxwell fluid over Riga plate, Sci. Iran. 28 (6) (2022) 3753–3766, https://doi.org/10.1177/1687814020968322.

[12] B. Ishtiaq, A. Zidan, S. Nadeem, M. Kbiri, Analysis of entropy generation in the nonlinear thermal radiative micropolar nanofluid flow towards a stagnation point with catalytic effects, Phys. Scr. (2022) 97, https://doi.org/10.1088/1402-4896/ac79d7.

[13] W.K. Usafzai, A. Emad, T. Marwa, A.M. Mahros, Modeling of micropolar nanofluid flow over flat surface with slip velocity and heat transfer: exact multiple solutions, Alexandria Eng. J. 75 (2023) 313–323, https://doi.org/10.1016/j.aej.2023.06.004.

[14] W.K. Usafzai, H.A. Emad, Exact multiple solutions of 2-D bidirectional moving plate micropolar hybrid nanofluid flow with heat transfer, Chin. J. Phys. 80 (2022) 414–426, https://doi.org/10.1016/j.cjph.2022.10.009.

[15] J.H. Merkin, I. Pop, Y.Y. Lok, T. Groşan, Similarity Solutions for the Boundary Layer Flow and Heat Transfer of Viscous Fluids, Nanofluids, Porous Media and Micropolar Fluids, Elsevier, Oxford, UK, 2021. https://www.sciencedirect.com/science/book/9780128211885.

[16] L.J. Crane, Flow past a stretching plate, Commun. Breves 21 (1970) 645–647, https://doi.org/10.1007/BF01587695.

[17] P.S. Gupta, A.S. Gupta, Heat and mass transfer on a stretching sheet with suction or blowing, Can. J. Chem. Eng. 55 (1977) 744–746, https://doi.org/10.1002/cjce.5450550619.

[18] R.U. Haq, S. Nadeem, N.S. Akbar, Z.H. Khan, Buoyancy and radiation effect on stagnation point flow of micropolar nanofluid along a vertically convective stretching surface, IEEE Trans. Nanotechnol. 14 (1) (2014) 42–50, https://doi.org/10.1109/TNANO.2014.2363684.

[19] M. Ashraf, S. Bashir, Numerical simulation of MHD stagnation point flow and heat transfer of a micropolar fluid towards a heated shrinking sheet, Int. J. Numer. Methods Fluids 69 (2) (2012) 384–398, https://doi.org/10.1002/fld.2564.

[20] M. Turkyilmazoglu, Flow of a micropolar fluid due to a porous stretching sheet and heat transfer, Int. J. Non Linear Mech. 83 (2016) 59–64, https://doi.org/10.1016/j.ijnonlinmec.2016.04.004.

[21] M.A. Sheremet, I. Pop, A. Ishak, Time dependent natural convection of micropolar fluid in a wavy triangular cavity, Int. J. Heat Mass Transf. 105 (2017) 610–622, https://doi.org/10.1016/j.ijheatmasstransfer.2016.09.044.

[22] U.S. Mahabaleshwar, K.R. Nagaraju, M.N. Nadagouda, R. Bennacer, D. Baleanu, An MHD viscous liquid stagnation point flow and heat transfer with thermal radiation and transpiration, J. Therm. Sci. Eng. Prog. 16 (2020) 100379, https://doi.org/10.1016/j.tsep.2019.100379.

[23] U.S. Mahabaleshwar, K.R. Nagaraju, M.A. Sheremet, E. Baleanu, E. Lorenzini, Mass transpiration on Newtonian flow over a porous stretching/shrinking sheet with slip, Chin, J. Phys. 63 (2020) 130–137, https://doi.org/10.1016/j.cjph.2019.11.016.

[24] A.J. Chamkha, M. Jaradat, I. Pop, Three dimensional micropolar flow due to stretching flat surface, Int. J. Fluid Mech. Res. 30 (4) (2003) 357–366, https://doi.org/10.1615/interjfluidmechres.V30.I4.10.

[25] M.M. Bhatti, H.F. Öztop, R. Ellahi, E. SarrisI, M.H. Doranehgard, Insight into the investigation of diamond (C) and Silica (SiO2) nanoparticles suspended in water-based hybrid nanofluid with application in solar collector, J. Mol. Liq. 357 (2022) 119134, https://doi.org/10.1016/j.molliq.2022.119134.

[26] F. Selimefendigil, F. ÖztopH, Thermal management for conjugate heat transfer of curved solid conductive panel coupled with different cooling systems using non-Newtonian power law nanofluid applicable to photovoltaic panel systems, Int. J. Therm. Sci. 173 (2022) 107390, https://doi.org/10.1016/j.ijthermalsci.2021.107390.

[27] F. Selimefendigil, F. ÖztopH, Impacts of using an elastic fin on the phase change process under magnetic field during hybrid nanoliquid convection through a PCM-packed bed system, Inte. J. Mech. Sci. 216 (2022) 106958, https://doi.org/10.1016/j.ijmecsci.2021.106958.

[28] M.M Bhatti, S.M. Sait, R. Ellahi, M.A. Sheremet, H.F. Oztop, Thermal analysis and entropy generation of magnetic Eyring-Powell nanofluid with viscous dissipation in a wavy asymmetric channel, Int. J. Numer. Methods Heat Fluid Flow 33 (2023) 1609–1636, https://doi.org/10.1108/HFF-07-2022-0420.

[29] F. Selimefendigil, H.F. Öztop, Analysis of MHD mixed convection in a flexible walled and nanofluids filled lid-driven cavity with volumetric heat generation, Int. J. Mech. Sci. 118 (2016) 113–124, https://doi.org/10.1016/j.ijmecsci.2016.09.011.

[30] K. Singh Dwesh, Free convection with MWCNT/water nanofluid having varying aspect ratio of MWCNT nanoparticle in thermally undulated enclosures, Int. J. Mech. Sci. 178 (2020) 105626, https://doi.org/10.1016/j.ijmecsci.2020.105626.

[31] T.R. Vijaybabu, Influence of permeable circular body and CuO-H_2O Nanofluid on buoyancy-driven flow and entropy generation, Int. J. Mech. Sci. 166 (2020) 105240, https://doi.org/10.1016/j.ijmecsci.2019.105240.

[32] M. Satyaranjan, B. Mahanthesh, M. Joby, K.P. Pradyumma, Nonlinear radiation and cross-diffusion effects on the micropolar nanoliquid flow past a stretching sheet with an exponential heat source, Heat Transf. 50 (4) (2021) 3530–3546, https://doi.org/10.1002/htj.22039.

[33] K.P. Pradyumma, M.M. Bhatti, S.R. Mishra, M.A. Abbas, O. Anwar Beg, Mixed Convective-Radiative Dissipative Magnetized Micropolar Nanofluid Flow over a Stretching Surface in Porous Media with Double Stratification and Chemical Reaction Effects: aDM-Padé Computation, J. Math. (2022) 9888379, https://doi.org/10.1155/2022/9888379.

[34] K. Das, Slip effects on heat and mass transfer in MHD Micropolar fluid flow over an inclined plate with thermal radiation and chemical reaction, Int. J. Numer. Methods Fluids 70 (2012) 96–113, https://doi.org/10.1002/fld.2683.

[35] S.R. Mishra, S. Baag, D.K. Mohapatra, Chemical reaction and soret effects on hydromagnetic Micropolar fluid along a stretching sheet, Eng. Sci. Technol. 19 (2016) 1919–1928, https://doi.org/10.1016/j.jestch.2016.07.016.

[36] K. Bhattacharyya, G.C. Layek, Similarity solution of MHD boundary layer flow with diffusion and chemical reaction over a porous flat plate with suction/blowing, Meccanica 47 (2012) 1043–1048, https://doi.org/10.1007/s11012-011-9461-x.

[37] C.Y. Wang, Flow due to stretching boundary with partial slip—An exact solution of the Navier Stokes Equation, Chem. Eng. Sci. 57 (2002) 3745–3747, https://doi.org/10.1016/S0009-2509(02)00267-1.

[38] S. Mukhopadhyay, Slip effects on MHD boundary layer flow over an exponentially stretching sheet with suction/blowing and thermal radiation, Aim Shams Eng. J. 4 (2012) 485–491, https://doi.org/10.1016/j.asej.2012.10.007.

[39] H.I. Anderson, Slip flow past a stretching surface, Acta Mech. 158 (2002) 121–125, https://doi.org/10.1007/BF01463174.

[40] R.L. Devi, A. Neeraja, N.B. Reddy, Radiation effect on MHD slip flow past a stretching sheet with variable viscosity and heat source/sink, Int. J. Sci. Innovative Math. Res. 3 (2015) 8–17. https://www.arcjournals.org/pdfs/ijsimr/v3-i5/4.pdf.

[41] M.C. Kemparaju, M.C. Abel, M.M. Nandeppanavar, Heat transfer in MHD flow over a stretching sheet with velocity and thermal slip condition, Adv. Phys. Theor. Appl. 49 (2015) 25–33. https://api.semanticscholar.org/CorpusID:55697310.

[42] E.O. Fatunmbi, A. Adeniyan, Heat and mass transfer in MHD micropolar fluid flow over a stretching sheet with velocity and thermal slip conditions, Open J. Fluid Dyn. 8 (2) (2018). http://www.scirp.org/journal/ojfd.

[43] K.R. Nagaraju, U.S. Mahabaleshwar, M. Siddalingaprasad, S. Yahya, Diffusion of chemical reactive species in non-Newtonian liquid due to a porous stretching/shrinking sheet: brinkmann model, J. Porous Media 25 (9) (2022) 1–17, https://doi.org/10.1615/JPorMedia.2022041279.

[44] K.E. Aslani, U.S. Mahabaleshwar, S. Jitender, I.E. Sarris, Combined effect of radiation and inclined MHD flow of a micropolar fluid over a porous stretching/shrinking sheet with mass transpiration, Int. J. Appl. Comput. Math 7 (60) (2021), https://doi.org/10.1007/s40819-021-00987-7.

[45] S. Saleem, I.L. Animasuan, S.J. Yook, Q.M. Al-Mdallal, N.A. Shah, M. Faisal, Insight into the motion of water conveying three kinds of nanoparticles on a horizontal surface: significance of thermos-migration and Brownian motion of different nanoparticles, Surface and Interface Analysis 30 (7) (2022) 101854, https://doi.org/10.1016/j.surfin.2022.101854.

[46] A.B. Vishalakshi, G.P. Vanitha, U.S. Mahabaleshwar, T. Botmart, H.F. Oztop, A.H. Nidal, Hiemenz stagnation point flow of a ternary nanofluid and heat transfer due to porous stretching/shrinking sheet with brinkman model, J. Porous Media 27 (2) (2024), https://doi.org/10.1615/JPorMedia.2023047575.

[47] I.L. Animasaun, O.K. Koriko, K.S. Adegbie, H.A. Babatunde, R.O. Ibraheem, N. Sandeep, B. Mahanthesh, Comparative analysis between 36nm and 47nm alumina water nanofluid flows in the presence of hall effect, J. Therm. Anal. Calorim. 135 (2019) 873–886, https://doi.org/10.1007/s10973-018-7379-4.
[48] M. Sahu, J. Sarkar, Steady-state energetic and exergetic performances of single-phase natural circulation loop with hybrid nanofluids, J Heat Transfer 141 (8) (2019) 082401, https://doi.org/10.1115/1.4043819.
[49] N. Acharya, R. Bag, P.K. Kundu, Influence of Hall current on radiative nanofluid flow over a spinning disk:a hybrid approach, Phys. E: Low-Dimension. Syst. Nanostruct. 111 (2019) 103–112, https://doi.org/10.1016/j.physe.2019.03.006.
[50] S. Rosseland, Astrophysik and Atom-Theoretische Grundlagen, Springer, New York, 1931. www.tat.physik.uni-tuebingen.de.
[51] G. Ahmadi, Self similar solution of incompressible micropolar boundary layer flow over a semi-infinite plate, Int. J. Eng. Sci. 14 (1976) 639–646, https://doi.org/10.1016/0020-7225(76)90006-9.
[52] M. Turkyilmazoglu, A note on micropolar fluid flow and heat transfer over a porous shrinking sheet, Int. J. Heat Mass Transf. 72 (2014) 388–391, https://doi.org/10.1016/j.ijheatmasstransfer.2014.01.039.
[53] L.J. Crane, Flow past a stretching plate, Z. Angew. Math. Phys. 21 (4) (1970) 645–647, https://doi.org/10.1007/BF01587695.
[54] K.E. Aslani, U.S. Mahabaleshwar, S. Jitender, I.E. Sarris, Combined effect of radiation and inclined MHD flow of a micropolar fluid over a porous stretching/shrinking sheet with mass transpiration, Int. J. Appl. Comput. Math 7 (60) (2021), https://doi.org/10.1007/s40819-021-00987-7.
[55] K.R. Nagaraju, U.S. Mahabaleshwar, M. Siddalingaprasad, S. Yahya, Diffusion of chemical reactive species in non-Newtonian liquid due to a porous stretching/shrinking: brinkmann model, J. Porous Media 25 (9) (2022) 1–17, https://doi.org/10.1615/JPorMedia.2022041279.
[56] R. Nazar, N. Amin, D. Filip, I. Pop, Stagnation point flow of a micropolar fluid towards a stretching sheet, Int. J. Non. Linear Mech. 39 (7) (2004) 1227–1235, https://doi.org/10.1016/j.ijnonlinmec.2003.08.007.
[57] K. Zaimi, A. Ishak, I. Pop, Flow past a permeable stretching/shrinking sheet in a nanofluid using two-phase model, PLoS ONE 9 (11) (2014) e111743, https://doi.org/10.1371/journal.pone.0111743.
[58] J. Merkin, On dual solutions occurring in mixed convection in a porous medium, J. Eng. Math. 20 (2) (1986) 171–179, https://doi.org/10.1007/BF00042775.